

DESIGN OF A CREEP EXPERIMENT FOR SiC/SiC COMPOSITES IN HFIR - S. L. Hecht (Duke Engineering Hanford), M. L. Hamilton, R. H. Jones, G. E. Youngblood, and R. A. Schwartz (Pacific Northwest National Laboratory), and C. A. Lewinsohn (Associated Western Universities)

OBJECTIVE

The purpose of this work is to design an in-reactor creep experiment for composite materials.

SUMMARY

A new specimen was designed for performing in-reactor creep tests on composite materials, specifically on SiC/SiC composites. The design was tailored for irradiation at 800°C in a HFIR RB* position. The specimen comprises a composite cylinder loaded by a pressurized internal bladder that is made of Nb1Zr. The experiment was designed for approximately a one year irradiation.

INTRODUCTION

This report describes the pressurized cylinder experiment design and supporting analysis for in-reactor creep testing of silicon carbide (SiC/SiC) composites, which are under consideration for structural applications in proposed magnetic fusion reactor systems. Recent qualitative and estimated quantitative data suggest that there is a significant effect of irradiation on the creep of SiC/SiC, and hence it is an issue which needs to be addressed in the design of such structures. This experiment is designed to obtain "engineering" creep data which can be utilized in the design process.

A number of design concepts were considered and analyzed in the preliminary design phase. Some of these concepts were rejected on the basis of programmatic constraints, and others were rejected because of technical issues. The result of this "screening process" was a design (referred to as the "reference design") which has a high degree of confidence of success. A second alternative design also holds some promise and is briefly addressed.

This report describes the experiment, and provides supporting performance predictions. Nuclear physics (shielding-heat deposition), thermal and structural analyses which provide design support are provided.

EXPERIMENTAL OBJECTIVES AND METHODS

The goal of the experiment is to obtain irradiation creep data which is representative of design needs for the fusion reactor system. These are specimen irradiation doses of 5 to 10 dpa and irradiation temperatures of 500 to 1000°C. Stresses were chosen to best study mechanistic effects. Here, hoop stresses in the specimen are expected to be initially chosen below, near and above the matrix cracking strength.

The experiment is designed to go in the High Flux Isotope Reactor (HFIR) in a Large Removable Beryllium (RB*) mid-core location. The HFIR is assumed to be operating at 100 MW power at the time of the irradiation. The experiment is expected to remain in the reactor for approximately one year, i.e., 300 effective full power days (EFPD), to obtain the desired dose.

The design is based on an assumed irradiation at the most severe conditions, i.e., 300 EFPD at 1000°C and a specimen hoop stress of 150 MPa. Hence a considerable design margin is expected to exist in experiments with a less severe environment.

The experimental system, because of available space, also provides an irradiation testing environment for other passive SiC specimens, such as bend bars and fibers.

DESIGN

The reference design of the SiC creep experiment system consists of a SiC/SiC cylinder specimen with an associated specimen loading subsystem, passive SiC creep specimens, and a subcapsule (RB*) whose main function is to provide mechanical support and temperature control. The experimental components, which are not specimens, i.e., the RB* subcapsule and the specimen-loading subsystem, are referred to herein as the "test assembly." There are three sets of specimens in each RB* subcapsule, as shown in Figure 1. The RB* subcapsule fits inside a stainless steel HIFR RB* Irradiation Capsule (at power ID = 1.364 in., OD = 1.504 in.), with the radial clearance between these two capsules set to provide the desired temperature range (see thermal analysis section).

The RB* subcapsule has the function of positioning the specimen systems, and providing the thermal environment and backup structural restraint for the specimen loading system (see structural analysis section). This subcapsule is fabricated of Nb1Zr refractory alloy, and is of welded construction. The Nb1Zr was chosen for the combined high-temperature strength and ductility, and ease of fabricability (see alternative design section). This capsule has a central thermocouple tube and gas line feed through a tube welded to the end caps. The end caps provide positioning holes for the specimen systems and centering and temperature control of the capsule via a scallop ledge. The RB* subcapsule is filled with helium gas at atmospheric pressure.

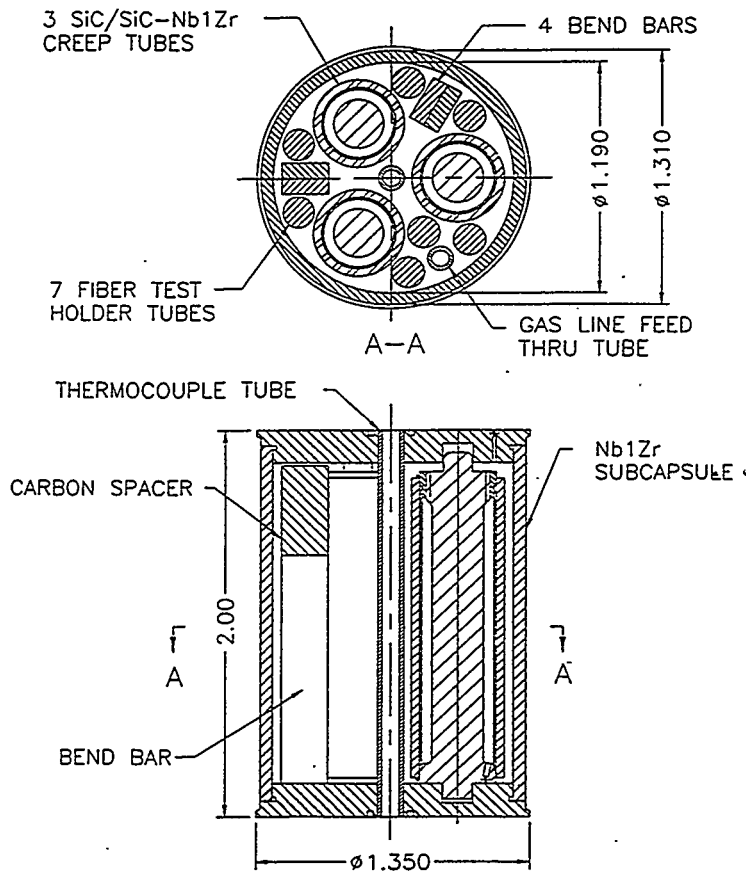


Figure 1 Layout of the RB* subcapsule. Dimensions given in inches.

The specimen loading system, also referred to as the SiC/SiC-Nb1Zr creep subcapsule, is shown along with the specimen cylinder in Figure 2. The main function of this system is to provide a fairly constant radial loading (pressure) to the SiC cylinder, which in turn, gives rise to a constant hoop stress in the specimen. The cylindrical specimen fits tightly on the loading subsystem (secured by pins) and is loaded from the thin-walled tubing (0.010 in. "bladder"). The outside of the bladder tube may be coated with a thin film (approximately 1 μm) of alumina to minimize any adverse chemical interactions between the Nb1Zr tube and the SiC cylinder. The center core and end cap components (with a threaded and welded ring at one end) minimize the axial deformation and axial load transmitted to the RB* subcapsule (see structural analysis section). This subsystem is constructed of all Nb1Zr. This material was chosen for the same reasons given above, plus it is the only refractory material for which irradiation creep data exist for the high temperatures of interest (see section on performance predictions). The gas space is filled with pressurized He gas. This pressure is set at room temperature so that at the operating temperature, the pressure is such that the desired hoop stress is produced in the specimen.

In addition to the test design described above, the experiment requires that a photon shield, most likely fabricated of depleted uranium, be inserted in the HFIR RB* location. This shield (ID = 1.66 in., OD = 1.92 in.) is an RB* position liner that fits around the RB* coolant channel, and reduces the gamma heating rates, as well as associated temperatures and temperature gradients in the specimen.

The experiment functions as follows:

1. As the reactor comes to power, gamma and neutron heating are generated within the RB* capsules.
2. This heat flows to the reactor coolant (outside the HFIR RB* irradiation capsule) via convection, conduction and radiation, creating temperature gradients within the capsules. To obtain the desired specimen temperature range, the annular control gas gap between the RB* capsule and the HFIR RB* irradiation capsule is set to a value determined in the design analysis. To compensate for uncertainties, the temperature can be "fined tuned" by adjusting the composition of the He/Ne gas mixture (RB* temperature control system) in the small annular temperature control gap.
3. Because of the increase in temperature over ambient conditions with the onset of irradiation, the preset pressure within the specimen loading system capsule increases (nominally according to the ideal gas law), which in turn imposes a radial pressure on the specimen cylinder. This radial pressure is reacting internally by a hoop stress within the

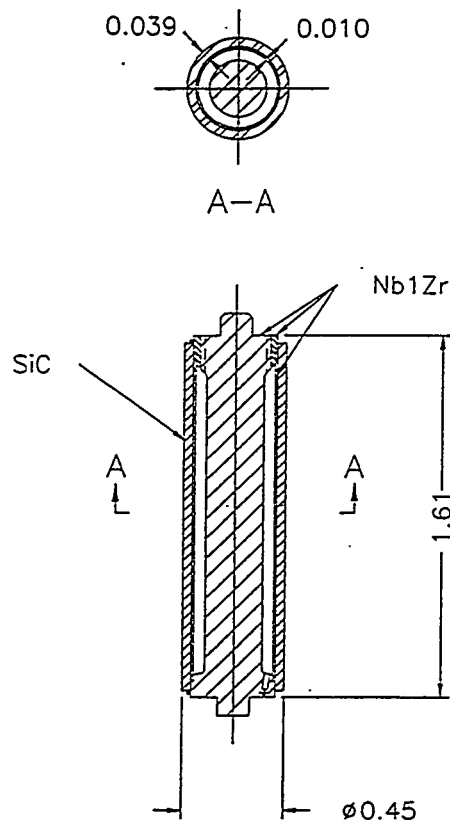


Figure 2 Schematic of creep specimen.

specimen. Differential thermal expansion causes an interference between the specimen and the bladder, but this is a secondary effect which relaxes out readily with irradiation.

4. The creep compliance in the thin Nb1Zr bladder tube is several orders of magnitude greater than that in the specimen, and in effect this tube "flows" with the specimen allowing the gas pressure to be transmitted radially to the specimen, with a minimum resistance of its own. Hence, during irradiation, a fairly constant hoop stress is maintained on the specimen, providing creep data at constant stress.

5. This thin-walled bladder tube is restrained in the axial direction both internally by the Nb1Zr core in the specimen loading subsystem and externally by the RB* subcapsule. This restraint mitigates the potential for stress rupture failure due to axial creep.

PERFORMANCE PREDICTIONS

Performance predictions were made to determine the time-dependent structural behavior of the pressurized cylinder specimen. The focus here was to get assurance that the objectives of the experiment could be met, and to provide a model which could be used in post-test data analysis. In the preliminary design phase, parametric studies were performed to improve the design and to assess sensitivities.

Finite element analysis (FEA) of the proposed experiment design modeled the pressurized Nb1Zr thin wall bladder tube, the SiC/SiC specimen cylinder (tube), and the interaction between the two tubes, at regions away from the end caps. The ANSYS FEA program (Swanson) was used for the two-dimensional (2-D) axisymmetric (R-Z) model using axisymmetric shell elements (SHELL51) for the tubes and gap elements (CONTAC12) for the frictionless interaction mechanics. The finite element model (FEM) only considers radial deformations, as axial friction between the bladder and the specimen is assumed to be nonexistent (see below). The model schematic is shown in Figure 3, giving element and node numbers.

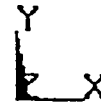
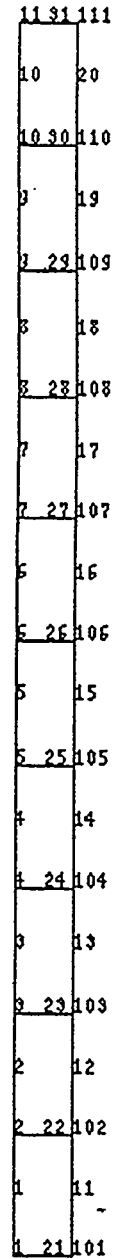
The model considered internal gas pressure loading on the bladder tube, thermal expansion of both tubes, irradiation creep of both tubes, and irradiation swelling of the Nb1Zr tube. Irradiation swelling the SiC/SiC cylinder was ignored as it is expected to be negligible. Because irradiation creep and swelling correlations did not exist for the Nb1Zr material at the temperatures of interest, relationships were developed using regression analysis on data given in the space power program literature (Paxton). Irradiation creep rates for the SiC composite were taken from Garner, et al., 1996. Other Nb1Zr material properties were taken from Carter, Hayes et al., and Garner et al., 1994. Neutron fluxes were assumed to be those for the HFIR reactor RB* location as given by Hobbs and Hicks. Analysis was made for the two main temperatures of interest, 800 and 1000°C. The corresponding room temperature pressures within the bladder tube were 8.95 and 7.26 MPa,¹ respectively, and were determined using an iterative procedure to produce a nominal initial 150 MPa specimen hoop stress at power.

Analysis of the reference design at 800 and 1000°C, in which there was an assumed small initial room temperature diametral gap of 0.02 mm (0.0008 in.), showed a small permanent increase in diameter of approximately 4.6 μm (a measurable value using existing equipment) at the end of 300 EFPD. The predicted deformations are comparable for both cases as the hoop stresses are equal and the creep rate is temperature independent for temperatures

¹SI and English units for pressure/stress are used interchangeably in this report. Both unit systems are not always cited; to convert psi to MPa multiply by 0.006896

below 1000°C. Figure 4 shows the calculated hoop stresses in both the SiC/SiC specimen and the bladder tube during the irradiation, for both temperature conditions analyzed. As shown, the hoop stress in the specimen remains nearly constant over the life of the experiment, a design goal.

At 1000°C, the calculated hoop stress in the specimen decreases 0.7% over 300 EFPD; for the 800°C case, the stress increases 3.1%. These differences can be explained, and are mainly due to the difference in thermal expansion interference (the Nb1Zr expands into the SiC/SiC). For irradiation at 1000°C, the hoop stress on the bladder tube is compressive, due to the combined effect of differential thermal expansion and internal pressure loading. As the interference compressive hoop stress on the bladder tube relaxes due to creep (the SiC/SiC specimen is dominant as its creep resistance is orders of magnitude greater than the Nb1Zr), the tube contracts, and hence, it causes a reduction of the interface pressure and the hoop stress in the specimen. As there is less interference at the 800°C conditions, the combined thermal and pressure effect produce a tensile hoop stress on the bladder, and hence has an opposite effect on the specimen. The hoop stress in the bladder in both cases significantly relaxes, and hence the bladder tube effectively transmits the internal pressure loading radially to the specimen with little internal resistance, as intended. This is confirmed as there is close agreement with the calculated hoop stress in the specimen using the thin wall treatment (pr/t) with the bladder pressure at power.



ANSYS 5.2
 MAR 12 1997
 08:43:29
 ELEMENTS
 ELEM NUM

ZV =1
 DIST=.006985
 XF =.004902
 YF =.00635
 Z-BUFFER

Figure 3 Schematic of FEM model, showing element and node numbers.

The uncertainty in friction between the coated Nb1Zr tube and the SiC/SiC specimen leads to an uncertainty in the stress state, and hence the effect on predictions versus measurement. The predictions assume a stress state which is uniaxial (hoop, θ). If friction exists along with negligible tangential creep in the bladder tube, then a biaxial stress state would exist in the specimen. The upper bound would be near a stress state for a pressurized closed tube, i.e., 2:1 (hoop to axial). Reality is likely to be a biaxial stress state somewhere in-between. This stress state should remain constant, unless

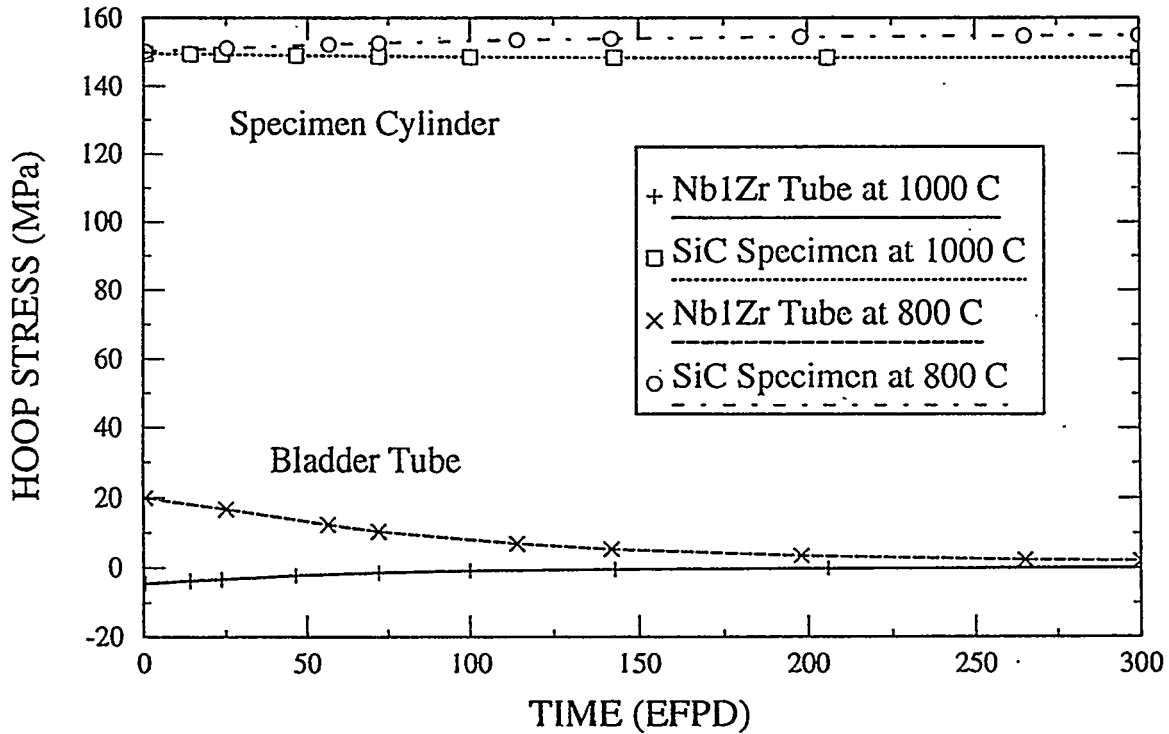


Figure 4 Calculated hoop stresses in SiC/SiC specimen and bladder tube during irradiation at 800 and 1000°C.

loading system "bottoms out" on the RB* capsule, in which case the axial strain increment is zero.

This uncertainty is expected to introduce at worst only a small error. Multiaxial stress state creep is based on the equivalent, or effective, stress and conservation of volume. The effective stress for this biaxial case is defined as:

$$\sigma_e = [(\sigma_\theta^2 + \sigma_a^2 + (\sigma_\theta - \sigma_a)^2) / 2]^{1/2}$$

For the case where the axial stress is 1/2 of the hoop stress, then:

$$\sigma_e = 0.866 \sigma_\theta$$

This says that there is an uncertainty range of creep deformation due to friction effects of no more than 13% (only the radial deformation is measured).

Sensitivity study cases were run for variations in Nb1Zr tube thickness, and irradiation creep and swelling rates to account for uncertainties. Calculations showed that reasonable uncertainties in the Nb1Zr material properties, including those due to irradiation swelling, did not have a significant effect on the resulting specimen stress and deformation. Small changes in the bladder wall thickness also did not have a significant effect on the specimen performance.

PHYSICS ANALYSIS

The purpose of this analysis was to determine the gamma ray heating rates for the material used in the SiC/SiC experiment and adjacent reactor components in a mid-core RB* location. The effects of different photon shield materials were also evaluated. These heating rates are used in subsequent thermal analysis.

The MCNP computer code (Breisemeister, Carter) was used for the heat deposition calculations. The calculation was made by modeling a cylinder containing regions for each of the different elements, i.e., concentric cylinders, as shown in Table 1. This model represents the photon shield (if included), the RB* coolant channel (water), the HFIR irradiation capsule, and the RB* subcapsule and internals. For this analysis it was assumed that the RB* subcapsule was constructed of TZM (see alternative design).

Table 1. MCNP Model Dimensions and Materials.

Radius (in.)	Shield	Density (g/cc)
0.25	Inner Void	0.0
0.28	Niobium	8.55
0.319	Carbon	2.62
0.358	Silicon	2.33
0.59	Helium	0.1787
0.625	Molybdenum	10.2
0.68	Helium	0.1787
0.75	Iron	7.86
0.83	Water	1.0
0.96	Shield (W/U)	19.3/18.9

The input files include an f6 heating tally to calculate the gamma heating. Because MCNP calculates the heat deposition as MeV/g, the heating tally was multiplied by $1.6022\text{E}-13$ W/MeV to convert to units of W/g.

The energy dependent gamma ray flux distribution used for these calculations is given in Table 2. The source was modeled in the MCNP calculation as four planes surrounding the metal element model. The source particles were emitted perpendicular to the different source planes. The total particle weight for the MCNP calculation was set equal to the total flux multiplied by the surface area of the four planes.

Table 3 summarizes the calculated heating rates for the various elements for cases of no shield, a uranium shield and a tungsten shield. As shown, the depleted uranium shield is the most effective in minimizing the heating rates, and hence was chosen as for the reference design.

Table 2. Gamma Ray Flux.

Energy (MeV)	Flux (photons/cm ² s ⁻¹)	
	PTP	RB*
0.00	0.00e+00	0.00e+00
0.50	7.80e+15	3.54e+15
1.00	1.85e+15	5.12e+14
1.50	8.52e+14	2.23e+14
2.00	3.72e+14	1.16e+14
2.50	3.39e+14	8.75e+13
3.00	1.51e+14	4.65e+13
4.00	1.55e+14	5.69e+13
5.00	1.14e+14	2.43e+13
20.00	9.27e+13	4.58e+13
Total	1.15e+16	4.65E+15

*From J. Gekin, ORNL.

Table 3. Heating Rates with Different Shields.

Element	No Shield (W/g)	Tungsten Shield (W/g)	Uranium Shield (W/g)
Nb	17.4	8.40	7.12
C	9.63	6.07	5.31
Si	10.5	6.50	5.71
He	9.42	5.78	5.04
Mo	18.6	8.13	6.90
He	9.43	5.57	4.84
Fe	13.1	6.47	5.63
Average (above)	12.6	6.70	5.79
Water	11.5	6.12	5.30
Shield		15.1	16.8

THERMAL ANALYSIS

The goal of the thermal design is to provide a design temperature (or temperature range) for the specimens. A secondary goal is to assure that the temperatures of structural members of the test assembly are acceptable. The thermal design includes the sizing of wall thicknesses, sizing of the control gas gap, and sizing of the scalloped centering rings on the RB* subcapsule end caps where much of the gamma heating occurs due to their thickness. The reduced gap at the end caps, in addition to providing a centering function, allows much of the heat to flow out of the RB* capsule without adversely affecting the temperature of the specimen.

Two 2-D finite element thermal analyses, an R-Z axisymmetric and a 2-D sector analysis, were made to determine the temperature distribution in the SiC/SiC specimens and test assembly. Both models use the ANSYS (Rev. 5.2) Finite element analysis program. These analyses considered internal heat generation due to gamma heating, conduction/convection within the specimen/bladder and capsule, thermal radiation across gas gaps, and convection to the reactor coolant. Material properties for these analyses were taken from Carter, CRC, Hayes et al., and Touloukin.

It is desirable, but not necessarily required, that all contents within the RB* subcapsule are at approximately the same test temperature (800 or 1000°C). The subcapsule is filled with helium gas for maximum heat transfer and uniformity in temperature. The Nb1Zr capsule wall and end caps provide much of the gamma heating to the subcapsule. The annular gas gap (Ne/He mixture) is used for temperature control. For design purposes, a nominal 50/50 mix of He and Ne is assumed. It is assumed that the ability to vary the gas mixture will compensate for any uncertainties in the analysis and reactor operations. Converging on a design, i.e., desired temperatures, was an iterative process involving varying the thickness of the subcapsule wall (within stress constraints), the annular gas gaps and the gas mixture.

The first thermal FEM, i.e., the R-Z axisymmetric model, is used primarily to size gas gaps and wall thicknesses. Resulting temperatures within the RB* subcapsule represent homogenized, or smeared, values only. One-dimensional models were not considered because of the axial effects (end cap gap and adjacent capsules). This R-Z axisymmetric FEM represents a one-half (axial symmetric centerline) axisymmetric section of the RB* subcapsule within the HFIR RB* irradiation capsule. Radially the model spans the RB* centerline to the reactor coolant. The FEM also simulates axial heat transfer to an adjacent cooler RB* subcapsule, which is expected to be the initial case, via pseudo axial gas gaps. The ANSYS model comprises axisymmetric ring conduction (PLANE55) elements, and radiation link (LINK31) elements which connect nodes on both side of the control gas gap.

This first FEM is shown schematically in Figure 5 (showing materials). The light blue color (#1) elements represent stainless steel components, e.g., the HFIR RB* irradiation capsule. The magenta color (#8) elements represent the He/Ne gas mixture in the temperature control gap. The red (#3) elements represent the Nb1Zr RB* subcapsule wall and end cap. The green (#6) elements represent the homogenized contents inside the RB* subcapsule. Here, volume weighted average properties and heat generation rates are used where the volume fractions are 54.1% He; 26.4% SiC; and 19.5% Nb1Zr. It was expected that the temperatures in the pressurized cylinder specimen and the specimen loading subsystem would likely be hotter than the maximum temperature predicted for homogenized treatment, and hence the design goal was set for a lower maximum predicted temperature (approximately 50°C). Material properties (thermal conductivity) are taken as temperature independent at an expected temperature range, and are given in Table 4. The effective emissivity used for the thermal radiation between the concentric stainless steel and Nb1Zr cylinders is 0.125. The convective heat transfer coefficient used for convection from the

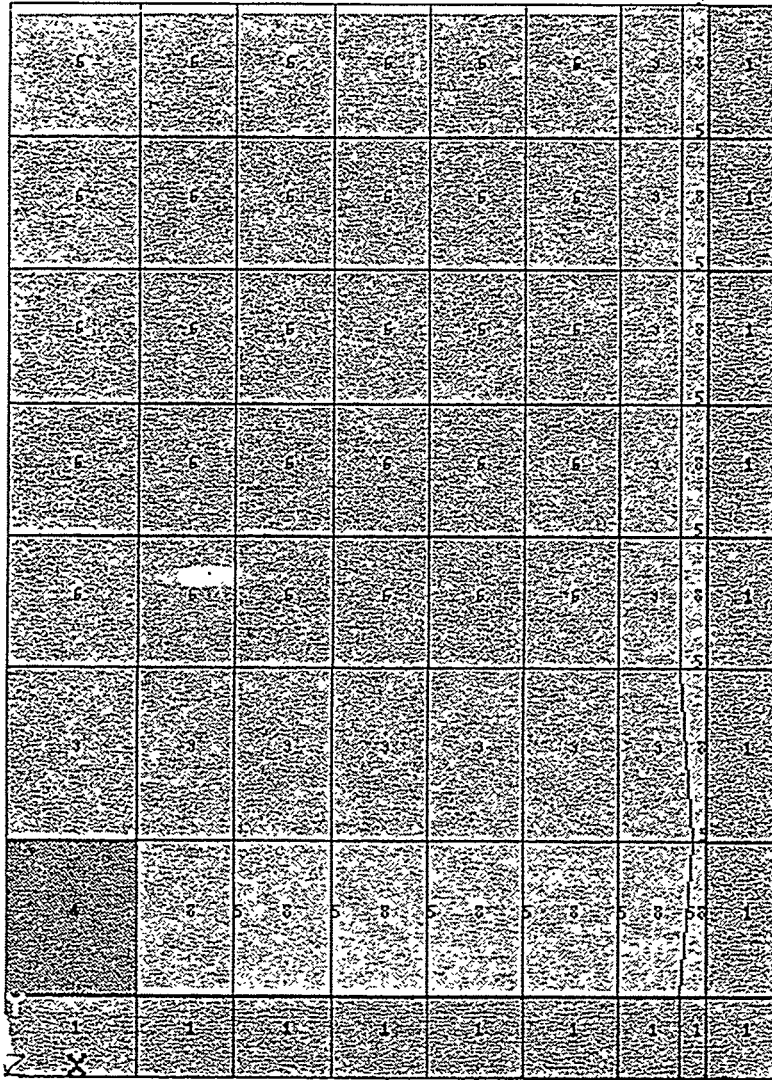


Figure 5 R-Z thermal FEM: materials/conductivity elements

convective heat transfer coefficient used for convection from the HFIR RB* irradiation capsule to reactor coolant (at 66°C) is 1935 Btu/hr-ft²-°C. This was determined via empirical relationships (Rohsenow, et al.) for forced convection for reactor coolant (water) flowing at 0.85 ft/s.

Figure 6 shows the resulting temperature profile for the 1000°C case. Here the maximum temperature in the HFIR RB* irradiation capsule is less than 200°C. The temperature drop across the control gas gap is approximately 650°C. The RB* capsule wall is at temperatures in the range of 870 to 890°C. An average 80°C temperature gradient is calculated within the RB* capsule, with a maximum average temperature of 950°C. The SiC/SiC cylinder specimen is expected to be at an average 1000°C. Similar trends were predicted for the 800°C design.

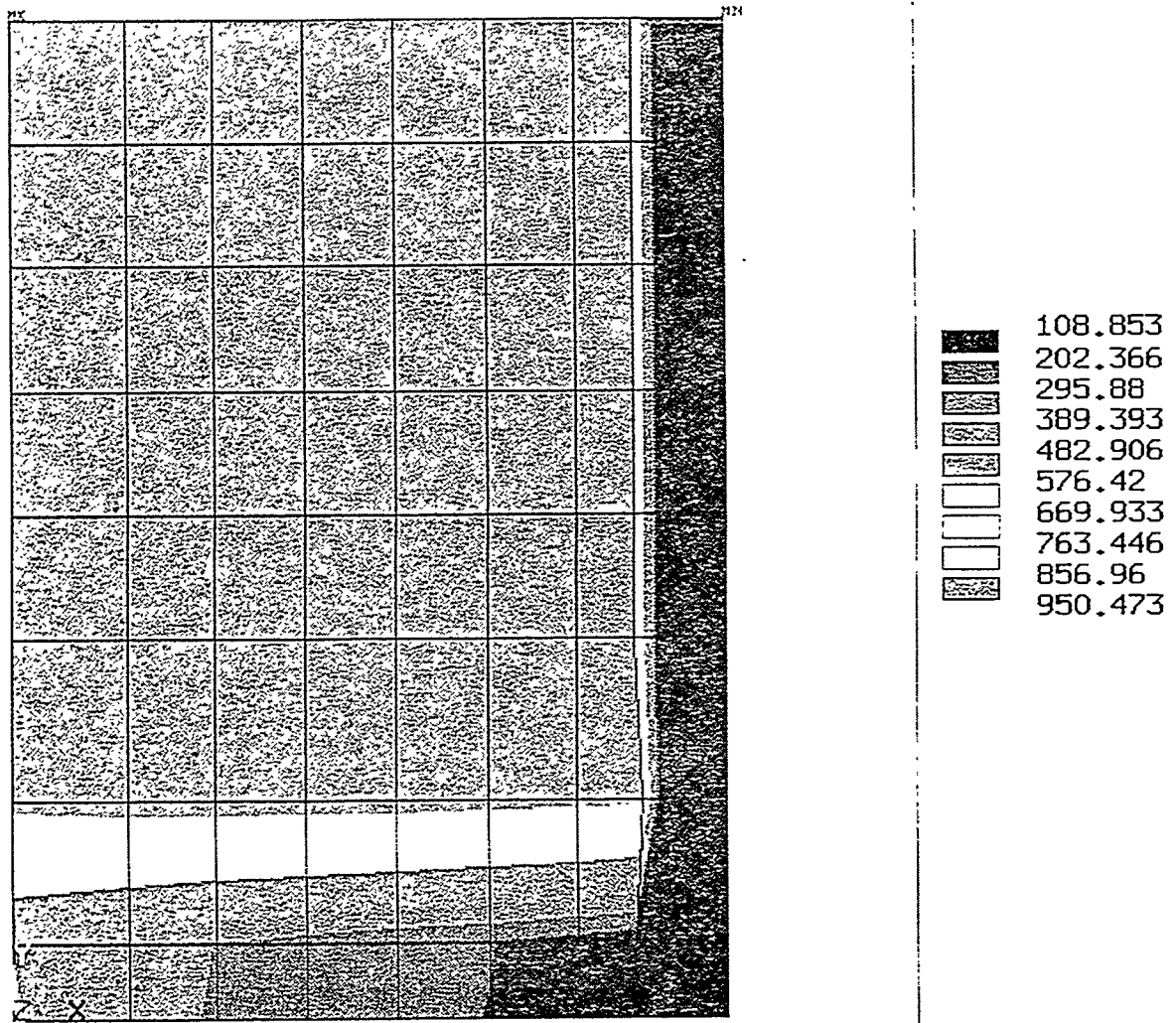


Figure 6 R-Z thermal FEM: temperature profile (1000°C case).

To obtain the desired temperature ranges, the following radial temperature control gaps (inches at power) are required:

	<u>800°C case</u>	<u>1000°C case</u>
Tube-to-tube:	0.019	0.027
Effective ¹ end cap to tube:	0.010	0.018

The second thermal FEM is designed to calculate more detail temperatures within the RB* subcapsule. This model (see Figures 7 and 8) is a 2-D 60° sector model (minimum section of symmetry) representing a slice through the axial center of the experiment. Regions from the thermocouple tube to the reactor coolant are modeled. As this model does not consider heat

¹As modeled minimum clearance; the actual geometry, i.e., the scalloped ridge, should have an equivalent thermal conduction characteristics.

flow in the axial directions, and is based on the tube-to-tube gaps, the resulting temperatures are expected to be higher than actual.

The model comprises ANSYS 2-D plane thermal conduction (PLANE55) elements and radiation link (LINK31) elements. Figure 7 shows the conduction elements with material numbering (colors and numbers). The light blue (#1) elements represent the stainless steel HFIR RB* Irradiation Capsule. The purple (#2) elements represent He gas in the bladder tube. The red (#3) elements represent the Nb1Zr components, which include the RB* Capsule tube, the thermocouple tube, and the bladder tube and core. The dark blue (#4) elements represent the SiC specimens and components. The magenta (#8) elements represent the control gas Ne/He 50/50 mixture. The yellow-green (#9) elements represent the He gas fill within the RB* subcapsule. The thermal conductivity, k , for this gas is an effective conductivity, k_{eff} , as it includes the effects of natural convection. This is considered reasonable as the gap is large enough for the existence of convection currents. k_{eff} is determined from empirical relationship summarized by Irwin, and effectively is 1.8 times larger than the normal conductivity of the gas itself. Radiation link elements are shown in Figure 8. Material properties (some of which are temperature dependent) are given in Table 5. Effective emissivities for material couples (assumes concentric cylinders with small annular gap for geometry) were 0.125 for Nb1Zr to Nb1Zr and Nb1Zr to stainless steel; and 0.14 for SiC to

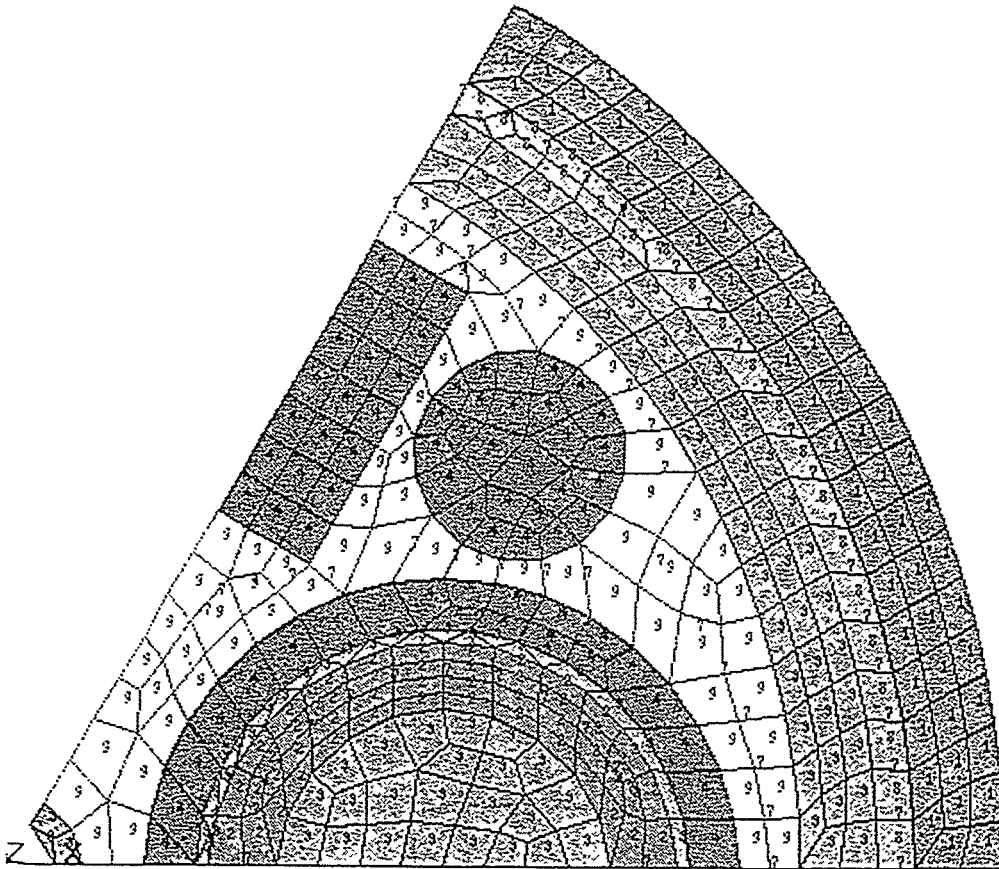


Figure 7 Sector thermal FEM: materials/conductivity elements.

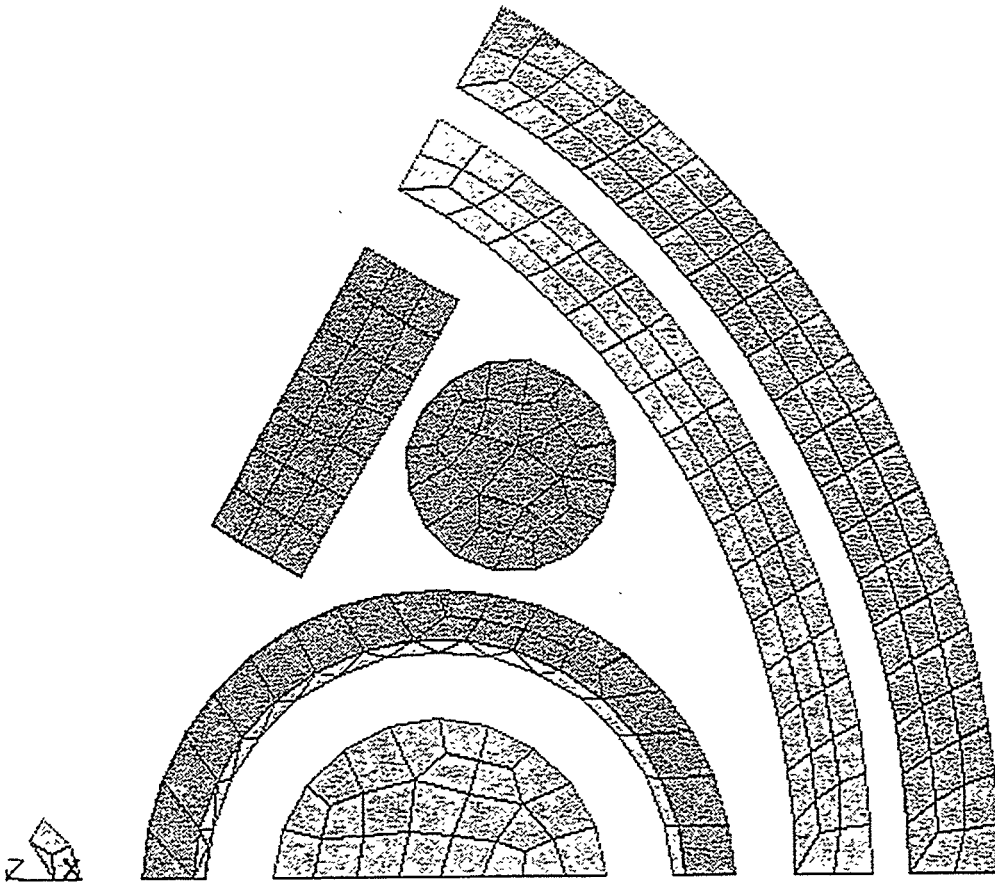


Figure 8 Sector thermal FEM: radiation link elements

SiC and SiC to Nb1Zr (Rohsenow, Touloukin). Predictions were made for the 1000°C case only, using the same annular control gap as was used in the R-Z analysis. Resulting temperature profiles are given in Figure 9 (overall profile) and 10 (internal RB* subcapsule). The overall profile shows that the temperature of the RB* subcapsule wall is about 170°C cooler than that predicted in the R-Z analysis, and that the gradient across the RB* capsule is 490°C, considerably more (as expected) than that predicted for the case with homogenized properties. When comparing the two cases, it is apparent that this sector model, which neglects the axial heat transfer effects, will overstate temperature gradients (axial effects and the thick end caps should mitigate the large ΔT s). It is likely that the RB* subcapsule wall will be hotter and that the specimen be cooler than is shown in Figures 9 and 10. Nevertheless, several conclusions can be drawn from these results. The thermocouple measurement may be as much as 80°C higher than the average cylinder specimen temperature. The temperature gradient around the circumference of the cylinder specimen may be as high as 150°C. The average temperature in the passive SiC specimens may be as much as 100°C cooler than the cylinder specimen. Temperature gradients across the bend bar and fiber test holder specimens may be up to 130 and 90°C, respectively.

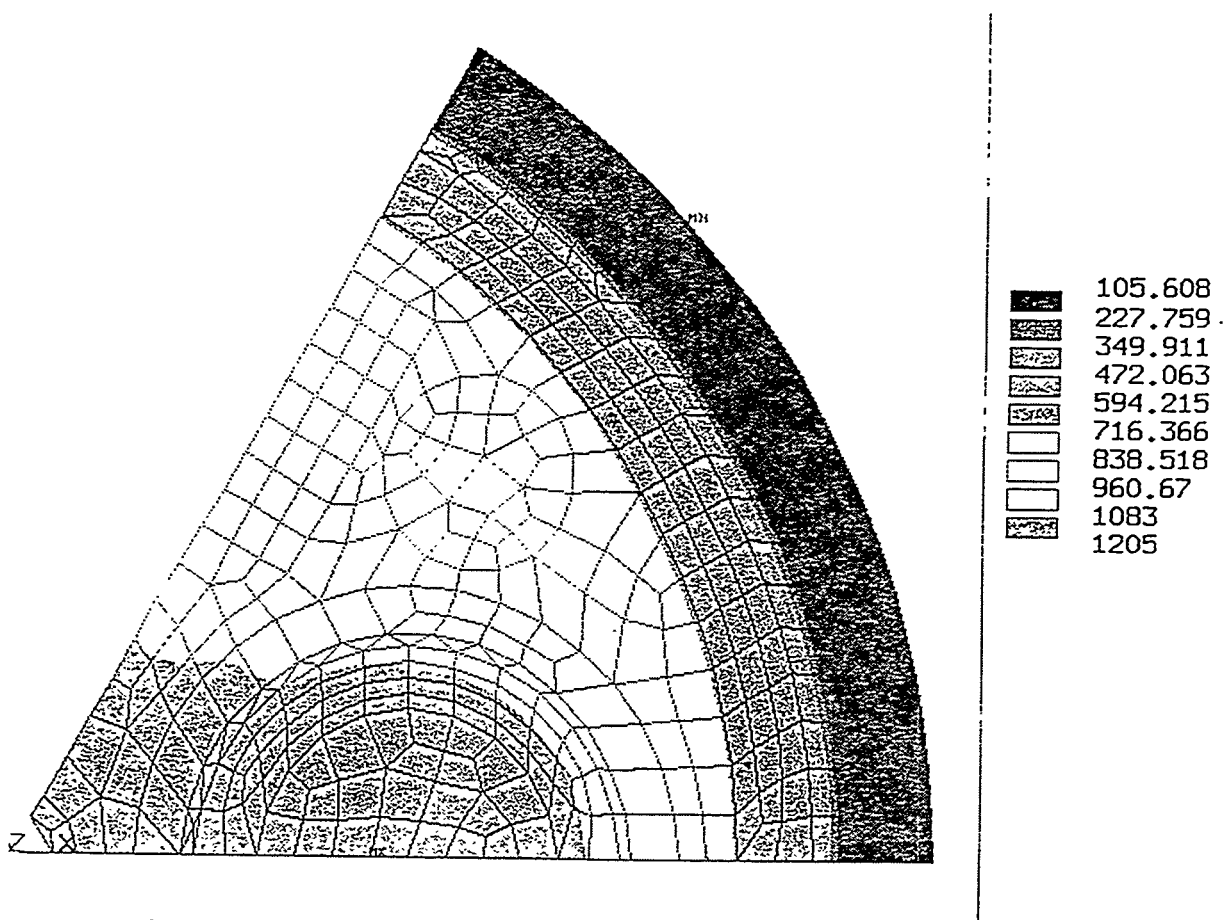


Figure 9 Overall temperature profile, 1000°C case.

Additional 2-D sector analyses were made to determine the effect of design options. One analysis assessed the control temperature range by varying the gas mixture. Here, pure He was used instead of the 50/50 Ne-He gas in the annular control gap. The results showed an 80°C change in average specimen temperature. Hence, the expected control range is 160°C or $\pm 80^\circ\text{C}$. Another design option (see alternative design section) considered a specimen loading system without a center core section. Here, the calculated circumferential temperature gradient was 100°C, as compared to 150°C in the reference design.

STRUCTURAL ANALYSIS

The structural analysis addresses the mechanical behavior and the structural integrity of the key components of the test assembly. This involves the calculation of stresses, strains, and deformations and their comparisons with failure criteria. The primary load on the system is from the internal gas pressure in specimen loading subsystem. Other loadings, which are secondary, are those due to differential thermal expansion. Loading due to differential swelling is not considered as the swelling gradients in the Nb1Zr are expected to be small (Garner et al., 1994, Wiffen).

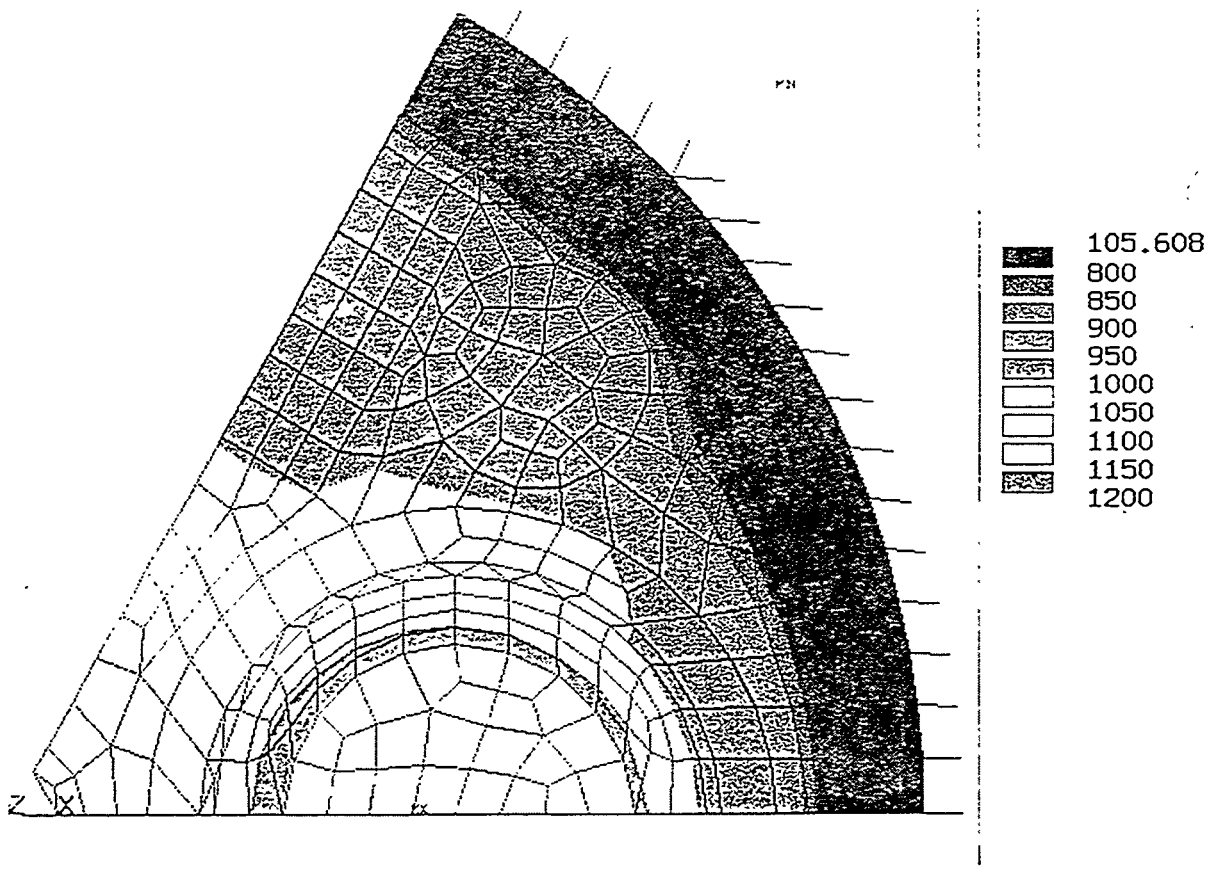


Figure 10 Internal subcapsule temperature profile for 1000°C case.

The specimen loading system is designed to resist the load from internal pressure on its own, i.e., without external support. For the 1000°C case, on which the design is based, the internal gas pressure increases from the room temperature value due to the increased temperature (the gas temperature is approximately 75 °C higher than the specimen) by a factor of $(1075 + 273)/(21 + 273) = 4.59$, to a pressure of 33.34 MPa. This pressure causes an axial force which is equal to this pressure multiplied by the cross-sectional area in the annular space between the bladder tube and the core. This force is reacted by the cross-sectional area of the bladder tube and the core, to produce an axial stress (F/A) of 26.59 MPa (note: this calculation conservatively neglects any resistance in the axial direction due to friction with the specimen). The radial force is reacted by the tube/specimen, which caused a secondary hoop stress in the bladder tube; these are given in the performance predictions section. As these hoop stresses are secondary (relax out) and are lower than the axial component, they need not be evaluated further, i.e., they are bounded. Discontinuity stresses in the bladder tube to end cap junction are not an issue as the deformations are restrained by the specimen.

The main concern for this component is that the axial stress will cause a stress rupture failure in the bladder tube/core. Stress rupture is evaluated via a Larson-Miller Parameter rupture curve as given in Figure 11 (Conway). For the estimated maximum temperature of the

bladder tube/core, 1100°C (2,472°R) and 300 EFPD (7,200 hr), the parameter $P = 2,472 \cdot [15 + \log(7,200)] = 4.66 \times 10^4$. From the curve in Figure 11 for the lower bound of the Nb1Zr data, the minimum stress to rupture is 29.5 MPa, which is greater than the operating stress of 26.6 MPa, and hence failure from stress rupture is not expected. Furthermore, for the 1000°C case, it is expected (see below) that the specimen loading system axially interacts with the RB* subcapsule due to creep, and hence the axial stress and corresponding creep damage on the bladder/core will be reduced.

The axial creep deformation in the specimen loading subsystem was also calculated. The analysis used a simple single element ANSYS model as ANSYS input data was previously set up for irradiation creep of Nb1Zr. Here a single ANSYS 2-D spar (LINK1) element of unit length and cross-sectional area was employed, so that the axial stress (26.6 MPa) is input as an axial force and the creep strain is calculated directly. Two cases were run: 1000 and 1100°C (the estimated temperature for the 1000°C specimen case). Creep strains of 0.98% and 5.2% were calculated at 300 EFPD for the 1000°C and 1100°C cases respectively. As the bladder tube length is 1.35 in., the creep deformations are 0.013 and 0.070 in. for the two respective temperature cases.

The axial clearance between the specimen loading system and the RB* subcapsule is 0.050 in., and hence for the 1000°C specimen case, axial interaction can be expected after approximately 210 EFPD (differential thermal expansion, with a 250°C ΔT , would close an additional 0.003 in.). For specimen temperatures lower than 1000°C, interaction is not expected.

Other secondary stresses in the specimen loading subsystem, which will relax out from creep, arise from the 100°C temperature difference between the hotter core and the bladder tube. To determine this thermal stress, we apply the conditions of equilibrium and compatibility and get the equation:

$$\alpha \Delta T_t l + F/k_t = \alpha \Delta T_c + F/k_c$$

where k (stiffness) = AE/l ; (l is length, A is cross-sectional area, E is the modulus of elasticity, α is the coefficient of thermal expansion, and the subscripts c and t refer to core and tube, respectively)

As l is equal, and assuming E and α are equal for the core and tube, we can solve for the interaction force (F). Here,

$$\begin{aligned} F &= \alpha E \Delta T_{ct} l / (1/A_c + 1/A_t) \\ &= (7.6 \times 10^{-6})(4.3 \times 10^6)(100) / (1/0.049 + 1/0.0113) = 30.0 \text{ lb} \end{aligned}$$

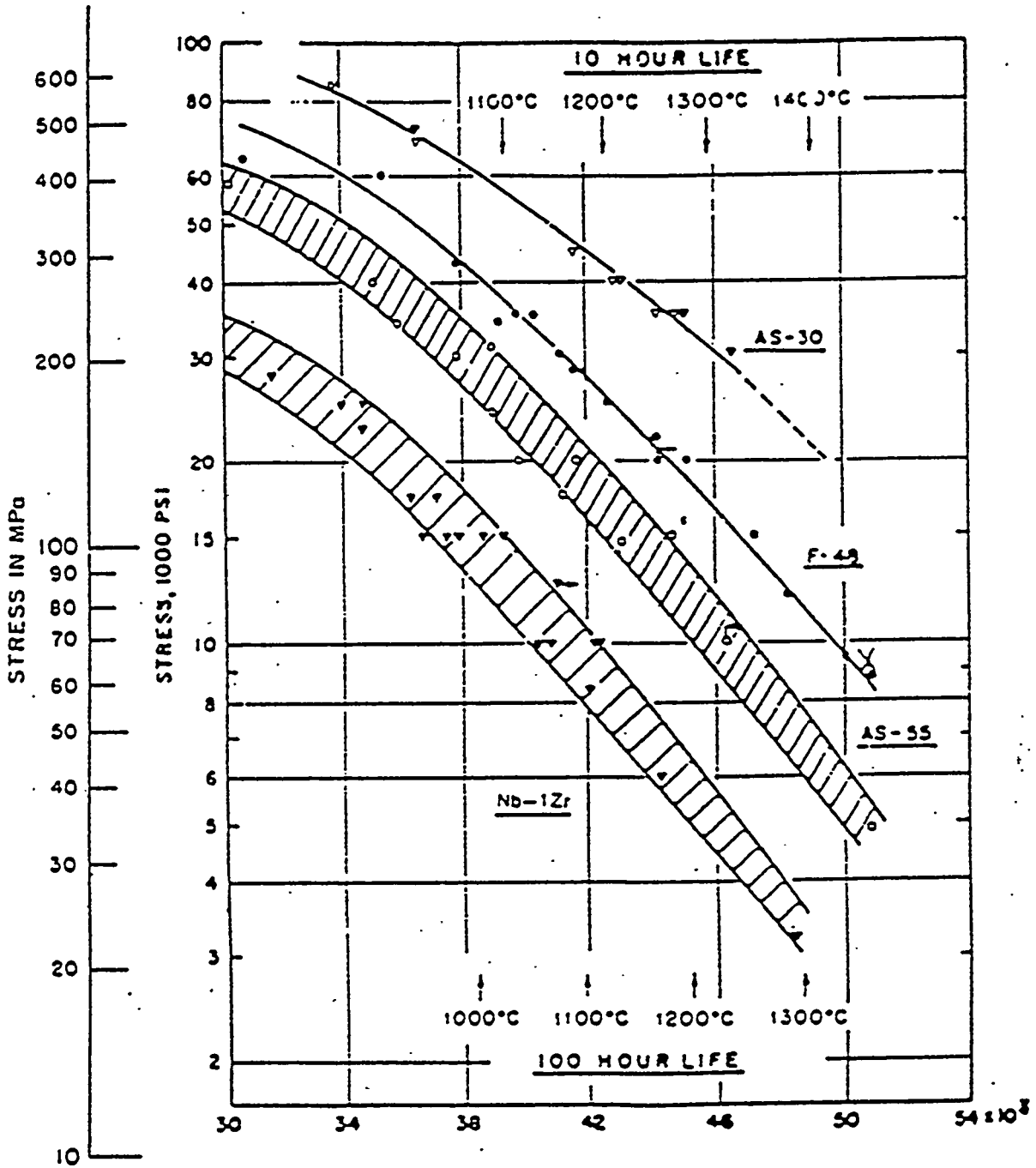
The corresponding stresses are:

$$\sigma_t = 30.0/0.0113 = 2,660 \text{ psi};$$

and

$$\sigma_c = -30.0/0.049 = -612 \text{ psi}$$

Primary loading and associated stresses on the RB* subcapsule arise from the above-mentioned interaction. The force produced by the bladder internal pressure is now reacted by the specimen loading system and the RB* subcapsule (in parallel). To determine the time-



$$P = T (15 + \log t_R); T^\circ R, t_R \text{ hrs}$$

Figure 11 Stress rupture strength of Nb-1Zr.

independent loading distribution, the relative stiffness, k , of these two load paths needs to be determined. This time-independent treatment shows that approximately 65% of the load is carried by the RB* subcapsule. When creep is involved, comparison of the inverse of the creep compliance needs to be addressed. For conservatism, it is assumed that all the load of 3,110 N (700 lb) from the three specimen loading systems is reacted by the RB* subcapsule. Assuming the stress is uniformly distributed to the end plates (see below), the axial primary membrane stress in the RB* capsule ($A = 0.235 \text{ in.}^2$) tube wall is $F/A = 700/0.235 = 2,980 \text{ psi}$ (this conservatively assumes that the thermocouple tube does not carry any of the load (see below). The primary (bending) principal stress in the end caps circular plate (thickness = 0.170 in.) as given by Griffel for a case where the outer edge is fixed and supported and the inner edge (thermocouple tube) is fixed, is:

$$\text{at the center: } \sigma_{r,t} = K_1 W/t^2 = (0.192)(700)/(0.17)^2 = 4,650 \text{ psi}$$

$$\text{at the edge: } \sigma_r = K_2 W/t^2 = (0.221)(700)/(0.17)^2 = 5,350 \text{ psi}$$

This closed form theoretical solution is conservative in that the thermocouple tube is free to float (rotation fixed). To better assess the stresses here and also to determine the load distribution on the circumference, which is needed for subsequent discontinuity analysis, and to address the actual loading, an FEA was performed. The ALGOR FEA program (Algor, Hecht) using three and four node Plate/Shell (Type 6) elements were used. This 60° sector (minimum section of symmetry) model is shown in Figure 12. Loading was applied as a pressure load on the region where the specimen loading system interacts with the RB* subcapsule. Both the full thickness of 0.170 in. and the reduced section, where the peg from the specimen loading system fits in the end cap, are modeled. Displacement boundary conditions were used for the fixed condition at the edge and the thermocouple joint. Appropriate boundary conditions, along with the use of boundary elements (on the 60° line) were employed to give symmetry conditions.

The calculated stress intensity profile (maximum difference of principal stresses) on the end cap is shown in Figure 12 (deformed shape stress plot). The maximum stress intensity at the center and edge are 1,790 and 1,420 psi, respectively. On the outer edge the bending stress varies by $\pm 43\%$ from an average value.

To determine this discontinuity stress including effects of stress concentrations (peak stress) an elastic FEA was used. Here, one-half symmetrical section of the RB* subcapsule (end cap and tube) was modeled. The model also included the central thermocouple tube, as it also provides axial support. The weld regions (weld preps) were modeled in detail to accurately treat stress concentrations, and calculate peak stresses. This FEM is an R-Z axisymmetric model as shown in Figure 13. Here the ALGOR program using both triangular and quadrilateral 2-D axisymmetric Solid Elasticity Elements (Type 4) was used. A very fine mesh was used in regions of stress concentrations. Loading was input as a constant pressure on the inside surface of the end cap.

Figure 13 shows the maximum principal stress (very close to stress intensity values) profile. The maximum peak principal stress of 16,800 psi is calculated at the root of the weld for the thermocouple. When considering the effect of the circumferential loading distribution, as determined on the end cap load analysis, the maximum peak principal stress in the root of the weld between the tube and the end caps is $(1.43)(12,400) = 17,700 \text{ psi}$. The maximum

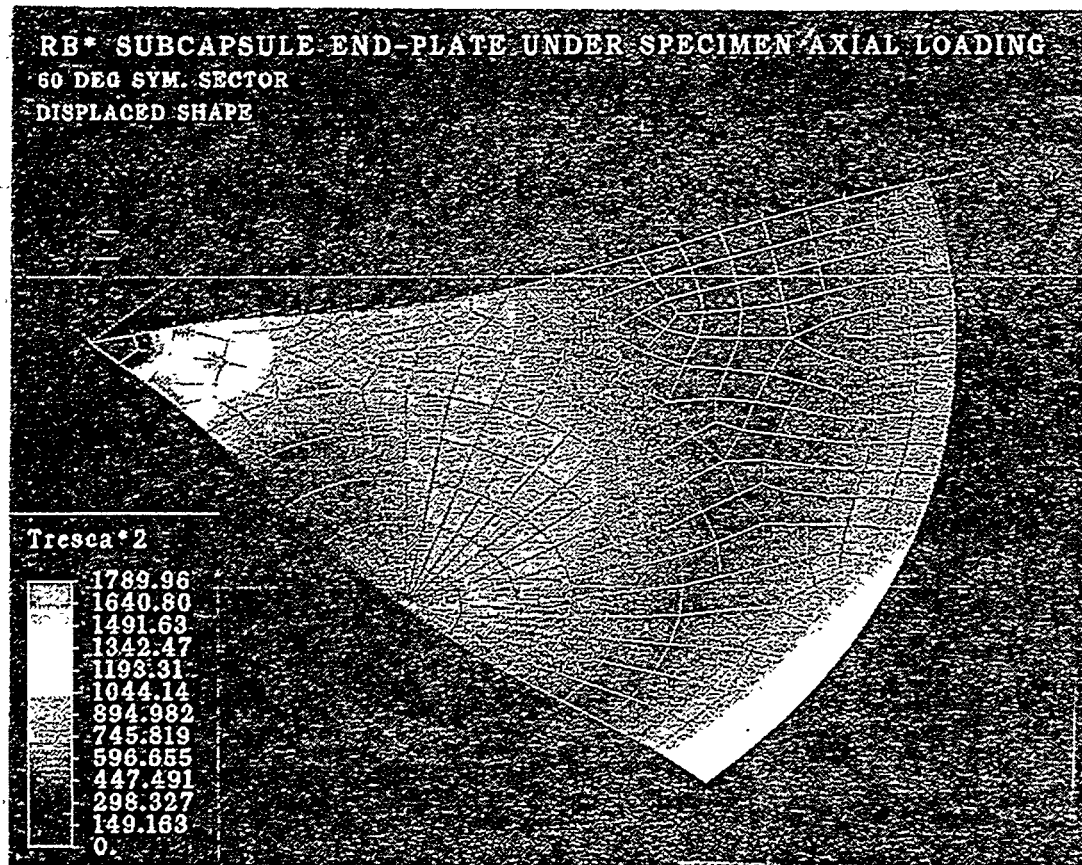


Figure 12 Stress distributino in 60° sector.

stress intensity, not considering stress concentrations, due to structural discontinuity is approximately $(2,340)(1.43) = 3,350$ psi at the junction of the tube and end cap.

The results show that the maximum axial membrane primary stress in the thermocouple tube is 10,200 psi (70.3 MPa). This is fairly high stress when considering stress rupture at the 1080°C thermocouple tube temperature. For the 90 EFPD time when the primary stress is expected to occur, the Larson-Miller parameter, P , is equal to 4.46×10^4 (see Figure 11). Stress rupture failures would not be expected at effective stress values below 6,000 psi (lower bound of the curve), and hence the current design is not acceptable. However some simple design fixes would provide an acceptable design. For example, increasing the thermocouple tube wall thickness from the current 0.040 to 0.065 in., will reduce the axial stress to 5,200 psi, an acceptable value. Additional design changes, such as increasing the axial clearance between the specimen load system and the RB* subcapsules, from the current 0.050 in., will also mitigate the above concern.

Secondary stresses are also produced from differential thermal expansion. Two areas need to be addressed here. The first is a temperature gradient across the RB* subcapsule tube

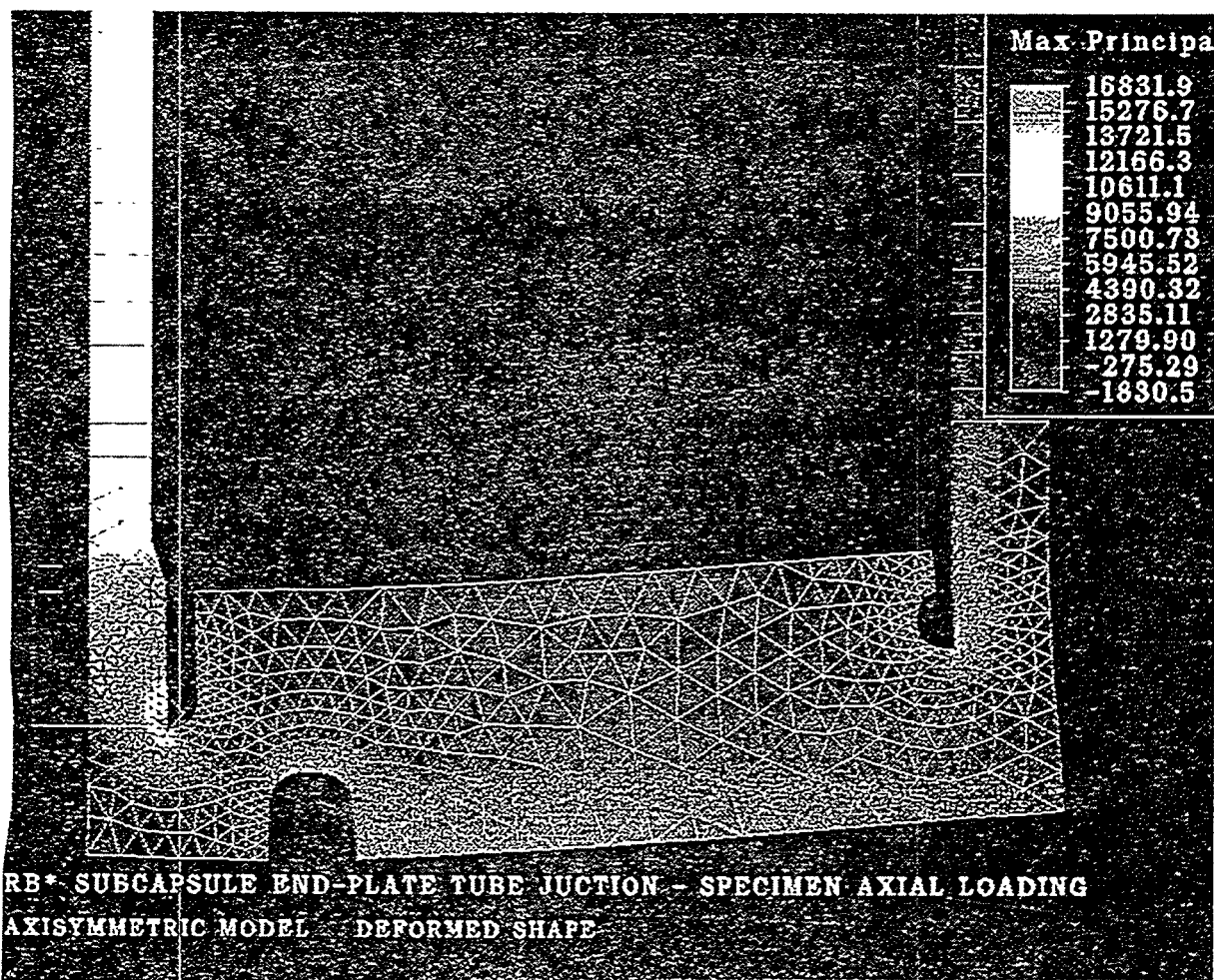


Figure 13 Axisymmetric model of the end cap/tube junction.

wall, where the maximum ΔT was calculated at 1000°C . The elastic bending stress due to the temperature gradient across the wall is:

$$\sigma = E\alpha\Delta T/[2(1-\nu)] = 0.857 \text{ MPa (125 psi)}.$$

Other thermal stresses are those due to temperature differential between the thermocouple tube (1080°C), the end cap and the capsule tube (850°C). To determine these stresses, nodal temperatures were specified on the FEM used in the discontinuity stress evaluation (approximate temperature in the end cap). Two load steps were evaluated: thermal loading only; and thermal plus axial pressure loading.

The results of this analysis show that the thermal load tends to counteract the axial pressure load, with the combined effect being lower stresses than calculated for just the axial loading. The combined loading is only in existence for the 90 EFPD, or less, when axial contact from the specimen loading system occurs. The thermal loading has the effect of closing the weld prep gaps (inherent crack), whereas the pressure load tends to open the gaps. For this combined primary plus secondary load case the maximum stress on the thermocouple tube

is reduced to 5,900 psi. For the welds the peak principal stresses reduce to approximately 1,000 psi at the root of thermocouple weld, and to $(1.43)(10,800) = 15,400$ psi at the end cap to tube junction. The combined axial plus bending (due to end cap expansion) stress in the capsule tube is less than 1,000 psi. These thermal stresses will tend to relax due to creep. However upon thermal unloading these stress ranges will exist in an opposite sense, and are considered in fatigue evaluations.

Evaluation of the structural integrity of the specimen loading system (at 1050 to 1100°C) and the RB* subcapsule (at 850 to 1080°C) need also be considered for failure modes other than the stress rupture evaluation as given above. Here failure modes such as ductile rupture, fatigue, and ratchetting are considered.

The unirradiated yield strength, S_y , and ultimate strength, S_u , of Nb1Zr at the 850°C are 22,000 and 30,000 psi, respectively (Conway). Wiffen has shown that HFIR irradiation to 14 to 28 dpa (higher than the reference EOL conditions) increases S_y to 28,000 psi and S_u to 40,000 psi. Irradiated uniform and total elongations of 3 and 5% were reported by Wiffen for 800°C, indicating some ductile behavior.

At 1050 to 1100°C, irradiated Nb1Zr showed good ductility with total elongations approaching 10% and with irradiated strengths of 30,000 and 37,700 psi for yield and ultimate, respectively (Hoark, et al., 1994). The unirradiated strengths of 20,000 and 23,000 psi were reported by Conway.

For the specimen loading subsystem, the maximum primary membrane stress of 26.6 MPa (3,860 psi) is well below either the irradiated or unirradiated yield strength of Nb1Zr. Using the rule of the ASME Boiler and Pressure Vessel Code: Section III for Class 1 Nuclear Power Plant Components, this stress should not exceed the minimum of $S_y/3$ or $S_y/2$, or 7,670 psi (using the conservative unirradiated values). The maximum secondary stress of 2,600 psi combined with the primary stress of 3,860 or 6,460 psi, should not exceed three times the primary stress intensity limit, or 23,000 psi. As both these conditions are met, the structural integrity of the specimen loading system is assured to a high degree of confidence.

For the RB* subcapsule, the maximum primary stress intensity of 5,200 psi in the redesigned thermocouple tube (at 1080°C) is less than the 7,670 psi allowable. The maximum primary membrane plus bending stress intensity of 1,790 psi in the end cap (conservatively assumes a temperature of 1080°C) does not exceed the code allowable of 1.5 times the primary membrane stress intensity limit, or 11,500 psi. The RB* subcapsules maximum primary plus secondary stress intensity is the 4,900 psi stress on the thermocouple tube. As this value is less than that evaluated for the primary stress intensity, it need not be further evaluated. As the peak stress intensity of 17,700 psi at the end cap to tube junction weld is less than the yield strength of the weld material and the number of cycles are low (reactor start-ups and shut-downs), fatigue failure is not a concern. Hence, as all conditions are satisfied, there is a high degree of confidence of maintaining structural integrity of the RB* subcapsule.

DISCUSSION

The analysis given here shows that with a few minor changes, the reference design experiment meets the design objectives. There is a high probability for success of the experiment as the design margins related to structural integrity and uncertainties associated with environmental conditions and performance are acceptable. The main disadvantage of the reference design is that the temperature gradient in the cylinder specimen is larger than desired. It is expected that variations to the reference design would mitigate this undesirable condition. Design changes, such as using a thicker bladder tube (high thermal conductivity to

even out temperatures), and making the fiber tube holder out of Nb1Zr (higher heating in a region where the temperature needs to be higher) would reduce this temperature gradient.

It is recognized that there is uncertainty in the thermal analysis results due to both the modeling assumptions (as demonstrated by different results for different 2-D analysis), and the uncertainties in material thermophysical properties, particular emissivities. No attempt has been made here to quantify the uncertainties, however it is expected the flexibility in the temperature control system is sufficient to compensate for these. If greater assurance of meeting the desired temperature is needed, an argon-helium gas mixture could be used instead of the neon-helium mixture considered here. This change would significantly increase the control range. However, the use of argon gas, while feasible, is discouraged as argon activates during irradiation, and presents problems to HFIR reactor operation.

ALTERNATIVE DESIGN

An alternative test assembly design was also evaluated in this design process. This design uses an RB* subcapsule that was made entirely of TZM, and a Nb1Zr specimen loading subsystem without a core. The test assembly functions basically the same way. However, the mechanics of the test assembly are somewhat different. Here, the axial load from the pressurized specimen loading subsystem is resisted by the RB* subcapsule. This axial load is approximately a factor of two higher than in the reference design. The RB* subcapsule is stronger here than in the reference design as TZM has high temperature strength significantly greater than Nb1Zr (approximately 3.5 times stronger, Wiffen).

The main advantage of this design is that there is less gamma heating in the subcapsule, without a core in the loading subsystem, and hence the temperature gradient in the specimen is lower (~100°C). Another advantage is the design and fabrication of the specimen loading subsystem is simpler. The main disadvantage of this design is that the irradiated TZM weld material has been shown to have very low ductility at temperatures below the irradiation temperature, following irradiation; such conditions could occur during the creep test, e.g., when HFIR is shut down between reactor cycles. The design was such that peak stresses (at stress concentrations) were kept to approximately 70% of the yield strength. The consensus on this issue is that the inherent margin of safety in this design is not sufficient. Other disadvantages are that the fabrication of TZM (welding and machining) is both difficult and costly.

COMPUTER RUNS

ANSYS input and output computer files are temporarily stored on the Hanford Scientific and Engineering Computational Center (SECC) in the /home/v92627/ansys/SiC directory. The ALGOR data files are temporarily stored on machine nucdes2.rl.gov in the /home/v92627/fem2/sic directory. At the program conclusion or termination the relevant files are anticipated to be archived in an compressed UNIX TAR file sic.tar.Z on the Hanford Common File System (bluegate.rl.gov) in directory /v92627/fem.

REFERENCES

1. American Society of Mechanical Engineers, *ASME Boiler and Pressure Vessel Code - Section III: Rules for Construction of Nuclear Power Plant Components*, 1971 Edition.
2. Algor, Inc., 1994, *ALGOR Reference Manuals*, P/N 6000.401, 4300.405, Pittsburgh, Pennsylvania.

3. Breisemeister, J. F., Editor, 1993, *MCNP - A General Monte carlo Code N Particle Transport Code*, Version 4a, LA-12625, Los Alamos National Laboratory, Los Alamos, New Mexico.
4. Carter, L. L., 1996, *Certification of MCNP Version 4A for WHC Computer Platforms*, WHC-SD-MP-SWD-30001, Rev. 7, Westinghouse Hanford Company, Richland, Washington.
5. Carter, R. J., 1989, *Ceramic Matrix Composites: Physical Properties for SiC/SiC Laminates*, Du Pont, Newark, Delaware.
6. Conway, J. B., 1984, *Mechanical and Physical Properties of Refractory Metals and Alloys*, Proceeding from Symposium on Refractory Alloy Technology for Space Nuclear Power Applications, Oak Ridge, Tennessee, August 1983, CONF-8308130.
7. CRC, 1970, *Handbook and Tables for Applied Engineering Science*, Chemical Rubber Company, Cleveland, Ohio.
8. Garner, F. A., Youngblood, G. E. and Hamilton, M. L., 1996, "Review of Data on Irradiation Creep of Monolithic SiC," Fusion Material Semiannual Report.
9. Garner, F. A., L. R. Greenwood, and D. J. Edwards, 1994, *The Influence of Starting State on Neutron Induced Density Change Observed in Nb-1Zr and Mo-41Re at High Exposures*, Journal of Nuclear Materials 212-215 426-430.
10. Griffel, W., 1966, *Handbook of Formulas for Stress and Strain*, Ungar Publishing Co., New York, New York.
11. Hayes, S. L., D. J. Senor, J. K. Thomas, and K. L. Peddicord, 1989, *Properties Library for Space Nuclear Reactors, Version 1.0*, Advanced Nuclear Fuel Laboratory, Texas A&M University, ANFL-10-R.
12. Hecht, S. L., 1991, *ALGOR Computer Code QA*, WHC-SD-GN-CSWD-321, Rev. 0, Westinghouse Hanford Company, Richland, Washington.
13. Hoark, J. A., M. M. Paxton, and L. K. Egner, 1991, *Third Interim Report on the Mechanical Properties of Nb-1Zr*, ORNL/TM-11430.
14. Horak, J. A., M. L. Grossbeck, and M. M. Paxton, 1994, *Effects of High-Temperature Exposure to Vacuum, Lithium and Fast Neutron Radiation on the Tensile Properties of Nb-1Zr*, ORNL-6810.
15. Hobbs, R. W., 1994, *High Flux Isotope Reactor Experimenter's Guide*, Oak Ridge National Laboratory, ORNL/M-2303.
16. Hicks, G. R., B. H. Montgomery, K. R. Thoms, and C. D. West, 1986, *HFIR Irradiation Facilities Improvements - The HIFI Project*, Journal of Nuclear Materials 141-143 (1986) 1018-1024.
17. Irwin, J. J., 1995, *Thermal Analysis Methods for Safety Analysis Reports for Packaging*, WHC-SD-TP-RPT-005, Rev. 1, Westinghouse Hanford Company, Richland, Washington.

18. Paxton, M. M., 1993, *Nb-1Zr Pressurized Tube Creep Correlation at SP-100 Service Conditions*, WHC-SP-1014, Westinghouse Hanford Company, Richland, Washington.
19. Rohsenow, W. M., and J. P. Hartnett, 1973, *Handbook of Heat Transfer*, McGraw-Hill, New York, New York.
20. Swanson Analysis System, Inc, 1994, *ANSYS User's Manual, Rev. 5.1*, DN-R300:51, Houston, Pennsylvania.
21. Touloukin Y. S., and D. P. Dewitt, 1972, *Thermophysical Properties of Matter*, Plenum, New York, New York.
22. Wiffen, F. W., 1994, *Effects of Irradiation on Properties of Refractory Alloys with Emphasis on Space Power Reactor Applications*, Proceeding from Symposium on Refractory Alloy Technology for Space Nuclear Power Applications, Oak Ridge, Tennessee, August 1983, CONF-8308130.